ACS OMEGA

http://pubs.acs.org/journal/acsodf

Article

Energy Dispersion in Pyridinium−Water Nanodroplets upon Irradiation

Paul Bertier, Léo Lavy, Denis Comte, Linda Feketeová, Thibaud Salbaing, Toshiyuki Azuma, Florent Calvo, Bernadette Farizon, Michel Farizon,* and Tilmann D. Märk

Cite This: *ACS Omega* 2022, 7, 10235−10242

Read Online

ACCESS | Metrics & More | Article Recommendations

ABSTRACT: Postirradiation dissociation of molecular clusters has been mainly studied assuming energy redistribution in the entire cluster prior to the dissociation. Here, the evaporation of water molecules from out-of-equilibrium pyridinium−water cluster ions was investigated using the recently developed correlated ion and neutral time-of-flight (COINTOF) mass spectrometry technique in combination with a velocity-map imaging (VMI) device. This special setup enables the measurement of velocity distributions of the evaporated molecules upon high-velocity collisions with an argon atom. The distributions measured for pyridinium−water cluster ions are found to have two distinct components. Besides a low-velocity contribution, which corresponds to the statistical evaporation of water molecules after nearly complete redistribution of the excitation energy within the clusters, a high-velocity contribution is also found in which the molecules are evaporated before the energy redistribution is complete. These two different evaporation modes were previously observed and described for protonated water cluster ions. However, unlike in the case of pure water clusters, the low-velocity part of the distributions for pyridinium-doped water clusters is itself composed of two distinct Maxwell−Boltzmann distributions, indicating that evaporated molecules originate in this case from out-of-equilibrium processes. Statistical molecular dynamics simulations were performed to (i) understand the effects caused in the ensuing evaporation process by the various excitation modes at different initial cluster constituents and to (ii) simulate the distributions resulting from sequential evaporations. The presence of a hydrophobic impurity in water clusters is shown to impact water molecule evaporation due to the energy storage in the internal degrees of freedom of the impurity.

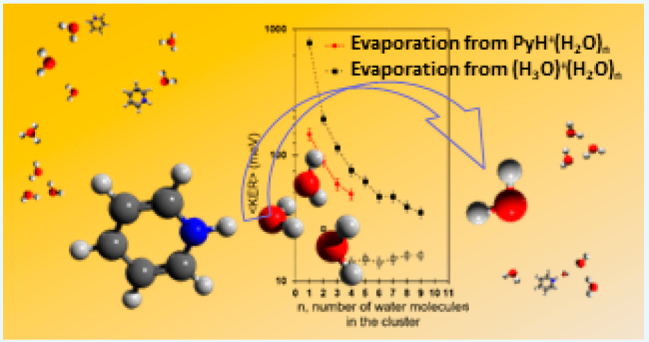

1. INTRODUCTION

Pyridine (C_5H_5N) is a hydrophobic aromatic molecule, and the pyridinium complex it forms with water has attracted significant attention in the scientific community owing to its importance in a broad range of fields, including atmospheric science and astrobiology. Pyridine is the raw material required to produce more complex nitrogen-substituted polycyclic aromatic hydrocarbons (NPAHs), and its presence in interstellar environments[1,2] contributes to questioning the origin of life on Earth, as prompted by the panspermia theory which supports that part of the material needed to generate life might originate from Space.[3] Investigations of the properties of pyridinium−water clusters have so far mainly focused on proton transfer mechanisms within the clusters[4−8] and on the propensity for hydrogen bonding[4,9,10] within a given time window, allowing the study of evaporation of molecules from clusters under equilibrium conditions. The recent development of the Dispositif d'Irradiation d'Agrégats Moléculaire (DIAM),[11] involving the correlated ion and neutral time-of-flight (COINTOF) mass spectrometer[12,13] combined with a velocity-map imaging (VMI) method,[14] gives us the opportunity to study the energy disposal in out-of-equilibrium molecular systems by measuring the velocity distribution of molecules evaporated from the cluster. The theories used to describe systems at equilibrium are well developed and allow the calculation of quantities such as temperatures or binding energies E_d from the kinetic energy released (KER). The framework developed by Klots[15] can notably be used to relate the width of the velocity distribution represented by the product of the molecule's temperature T and the Boltzmann constant k_B: k_BT to the binding energy E_d of the evaporated

Received: December 3, 2021
Accepted: March 4, 2022
Published: March 17, 2022

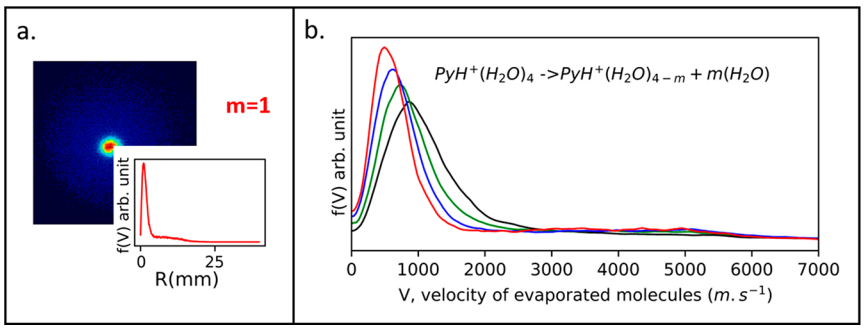

Figure 1. Impact and velocity distributions of water molecules evaporated from excited $PyH^+(H_2O)_4$ cluster ions. (a) 2D impact distribution of the evaporated molecules with its corresponding 1D integrated radial distribution for the evaporation of m = 1 water molecule (inset); (b) velocity distributions for dissociations involving one (red line), two (blue line), three (green line), or four (black line) evaporated water molecules.

molecule.[15] The first measurements of KER that could be used to measure E_d were performed on the decay of carbon dioxide cluster ions by Stace and Shukla.[16] These authors also investigated the statistical repartition of the excess energy in argon clusters before their evaporation.[17]

In the present contribution, we have studied the out-of-equilibrium evaporation of water molecules after electronic excitation of pyridinium−water cluster ions. Velocity distributions of evaporated molecules upon high-velocity collisions with an argon atom were measured, providing detailed insights into the energy transfer within the cluster. We find that the velocity distributions measured for pyridinium−water clusters have two distinct components. Besides a low-velocity contribution, which corresponds to the evaporation of a water molecule after nearly complete redistribution of the excitation energy within the cluster, a high-velocity contribution is also found in which the molecule is evaporated before the energy redistribution is completed. These two evaporation modes were previously identified in protonated water cluster ions.[18] However, unlike in pure water clusters, the low-velocity part of the velocity distributions for pyridinium-doped water clusters is itself composed of two distinct Maxwell−Boltzmann distributions, indicating that evaporated molecules in the low-velocity part also result from competing out-of-equilibrium processes. Moreover, the evaporation of water molecules from excited clusters is found to be much slower when the water cluster is doped with a pyridinium ion.

2. EXPERIMENTAL SETUP

The DIAM apparatus used here to generate a beam of energy- and mass-selected pyridinium−water cluster ions $PyH^+(H_2O)_n$ has been described elsewhere.[11,18] In summary, a neutral beam produced by a continuous supersonic expansion of a pyridine and water vapor is ionized by electron impact. The positive ions are accelerated to 8 keV and double focused by a $\vec{E} \times \vec{B}$ sector field mass spectrometer which selects the ions in energy and mass. Then, the $PyH^+(H_2O)_n$ ion beam collides with an effusive argon gas jet whose density is controlled to ensure single-collision conditions. After excitation by these collisions, the excited cluster ions will dissociate into a charged fragment and one or several neutral species. All fragments, neutral and charged, are then mass analyzed by the COINTOF technique described in detail elsewhere.[12−14,19,20]

The COINTOF technique allows correlated detection on a single detector of the neutral and charged fragments originating from the same single dissociation event. In short, the charged fragments are extracted from the collision region, accelerated proportionally to their mass-to-charge ratio (m/q), and enter a field-free region. The neutral fragments keep in principle the initial velocity of their parent ions, and their respective arrival time serves as an internal reference for each single-collision event. All fragments are then detected on a microchannel plate detector (MCP, F2225-21X from Hamamatsu) and the measurement of the arrival time of each fragment, i.e., the ion and at least one of the neutral counterparts, permits the identification of the charged species. A delay-line anode detector (DLA DLD40, Roentdek) located after the MCP detector associates coordinates (x and y) of the impact position on the detector of each fragment. The overall information, event by event, is saved to keep the correlation of the time and position information on all the fragments produced in a single-cluster ion dissociation. The intensity of the incident beam is kept below 500 counts per second to minimize the probability of detecting fragments produced from different decaying parent cluster ions.

After collision, the deposited energy possibly leads to the dissociation of the incident cluster ion. The KER upon dissociation is partitioned to the various fragments according to total momentum conservation. In the present study, we restrict our discussion only to dissociations leading to the loss of water molecules from the parent cluster ions. The evaporated molecules acquire an additional velocity randomly oriented in the center-of-mass reference frame (CMF) of the parent cluster. For the evaporated molecules, the additional velocity in the CMF leads to a transverse velocity component in the laboratory frame and consequently to a change in the impact position on the detection plane. The left part of Figure 1 shows the impact distributions for an 8 keV-$PyH^+(H_2O)_4$ incident beam in the x−y plane and the evaporation of a single water molecule. The impact distribution exhibits a clear radial symmetry, and thus the 2D distributions can be restricted to a 1D radially integrated distribution, also shown in the inset. The combination of an iterative unfolding technique based on the Bayes theorem and a Monte Carlo simulation of the detection device allows us to deduce the corresponding velocity distributions.[12,21] The velocity distributions corresponding to the four dissociation channels are represented in the right panel of Figure 1. All of them have two components: a peak between 0 and 2000 m s^{-1} and a large tail extending to 6000 m s^{-1}. The average value and the width of the lower part of the velocity distribution both increase with the number m = 1 to 4 of evaporated molecules.

https://doi.org/10.1021/acsomega.1c06842
ACS Omega 2022, 7, 10235−10242

3. RESULTS AND DISCUSSION

3.1. Evaporation of a Single Water Molecule.

3.1.1. Kinetic Energy Release. The energy deposited into the system during the collision lies typically in the range of 0–12 eV, and in around 80% of the cases it falls below 4 eV.[22] This energy is therefore in most cases above the intermolecular dissociation energy of the water molecules or the pyridinium molecular ion in the cluster, which ranges between 0.3 and 0.7 eV for the $PyH^+(H_2O)_{n=1-4}$ cluster ions.[23,24] We focus first on the evaporation of a single water molecule. The velocity distributions for the evaporation of a single molecule induced by collision of 8 keV-$PyH^+(H_2O)_{n=1-4}$ cluster ions with argon atoms are shown in the first column of Figure 2 as a function of cluster size n. The experimental distributions exhibit two distinct contributions: a low-velocity component between 0 and 2000 m s^{-1} and a high-velocity component between 2000 m s^{-1} and 6000 m s^{-1}.

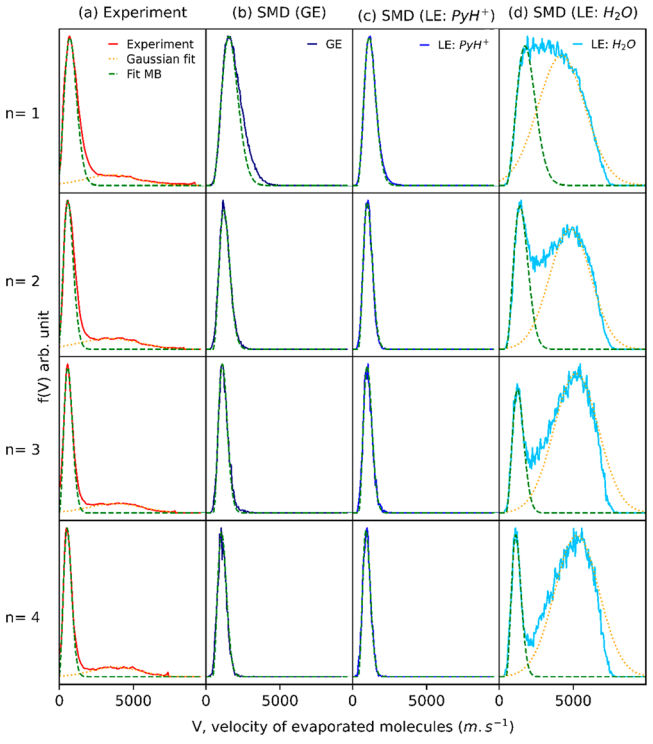

Figure 2. Velocity distributions obtained from the evaporation of a single water molecule from $PyH^+(H_2O)_{n=1-4}$ cluster ions. Experimental distributions are shown in the first column (a). Simulated distributions obtained from statistical molecular dynamics (SMD) shown correspond to global excitations (GE, column (b)), to a local excitation of the pyridinium ion (LE: PyH^+, column (c)), or to a local excitation of a random water molecule (LE: H_2O, column (d)). The dashed green curves correspond to Maxwell–Boltzmann fits of the low-velocity part of the distributions, and the dashed orange curves correspond to Gaussian fits of the high-velocity nonergodic events.

Such a behavior is similar to the one observed earlier in collision induced dissociation (CID) experiments on protonated water cluster ions.[25] These previous results showed that the low-velocity part can be fitted very well with a Maxwell–Boltzmann distribution and therefore represents thermalized parent ions in which the deposited energy was statistically redistributed among all vibrational modes before dissociation. The corresponding fragmentation events will be referred to as Maxwell–Boltzmann events. Moreover, a high-velocity contribution was also observed in these CID experiments on protonated water cluster ions, corresponding to nonergodic evaporations of water molecules before complete energy redistribution in the droplet.[25]

The total kinetic energy release (KER) during the dissociation is extracted from the low-velocity part of these distributions. The velocity of the evaporated molecule is directly related to the KER, whose averaged value can be calculated by using the momentum and energy conservation laws:

$$\langle \mathrm{KER} \rangle = \frac{1}{2} m_{H_2O} \langle V^2 \rangle \left(\frac{m_{H_2O}}{m_{ion}} + 1 \right) \quad (1)$$

with V the velocity of the evaporated water molecule, and m_{H_2O} its mass.

The values obtained for the average total KER are presented in Figure 3 as a function of cluster size n. For comparison, the ⟨KER⟩ obtained for neat protonated water clusters measured under the same experimental conditions is also shown in Figure 3. In both cases, the ⟨KER⟩ is found to decrease strongly with increasing n, and similar values are reached for pyridinium-doped and protonated water clusters at large n. Small nanodroplets are stabilized by the strong intermolecular bonds created by the proton, but the charge's role decreases rapidly with increasing numbers of water molecules. For nanodroplets containing a larger number of water molecules, the properties are determined by these molecules, and the individual role of the ion (H_3O^+ or PyH^+) becomes negligible. We notice that in the case n = 1 only two molecules are connected by an intermediate proton. This result is in

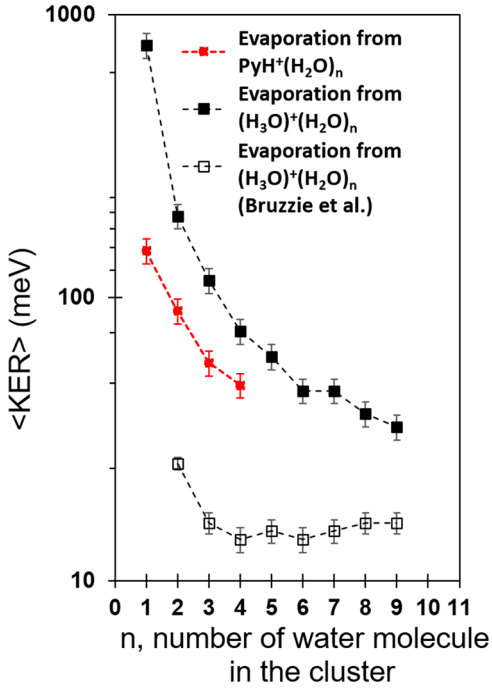

Figure 3. Mean value of the total KER deduced from the low-velocity part of the velocity distributions measured in this work for $PyH^+(H_2O)_{n=1-4}$ cluster ions (present work: closed red square). For comparison, the results for $H_3O^+(H_2O)_n$ cluster ions obtained with the same setup (closed black squares[21]) and from Bruzzie et al.[27] (open black squares) are also reported.

https://doi.org/10.1021/acsomega.1c06842
ACS Omega 2022, 7, 10235–10242

agreement with computational studies performed by Caleman and Van Der Spoel[26] on the evaporation from larger water clusters containing 216 or 512 molecules that showed that ions present and forming hydrogen bonds do not affect the evaporation significantly compared to a pure water cluster.

Moreover, Figure 3 also shows the results for ⟨KER⟩ measured by Bruzzie, Parajuli, and Stace[27] for the evaporation of a molecule from metastable cluster ions $H_3O^+(H_2O)_{n=2-29}$. The reported ⟨KER⟩ values are much smaller than the present ones and show no dependence on size above a cluster size of $n = 3$. In contrast to our experiment, these authors focused on the decay of metastable cluster ions over much longer time scales of about 10^{-4} s, hence probing much colder internal states.[27] In our experiment, the possible amount of energies deposited is quite broad (ranging from 0 to 12 eV) and can thus be above the amount of energy necessary to evaporate more than one molecule. Therefore, the shape of the velocity distribution is not limited by the energy deposition but results from the out-of-equilibrium dynamics: to be in the measured (size-selected) distribution, the out-of-equilibrium droplets must have evaporated one molecule during the observational time window but no more than one. With increasing deposited energy, several evaporation channels come into competition with each other, and the likelihood of evaporation of two or more molecules thereby increases. This competition originates from the many pathways after redistribution of the excess energy into the various intermolecular degrees of freedom.

3.1.2. Modeling by Statistical Molecular Dynamics Simulations. The experimental velocity distributions are analyzed by dedicated computational modeling at the atomistic level of details, using as introduced earlier for protonated water clusters statistical molecular dynamics (SMD) simulations.[25] We use the nonpolarizable Amber *ff*99[28] potential to describe microhydrated pyridinium complexes and start by generating equilibrated configurations, in phase space, of various microhydrated complexes containing between 1 and 10 water molecules, although we focus below on a more restricted range. Replica-exchange molecular dynamics trajectories are used to generate these phase space samples, employing four temperatures allocated geometrically in the 50−150 K range. These trajectories consist of a thermalization period of 200 ps, followed by 1 ns proper sampling in which configurations (positions and velocities) are saved every 100 fs at the third trajectory with the temperature close to 100 K. The standard Nosé−Hoover thermostat method is used for this thermalization part, all simulations being performed using homemade codes. Then random configurations are chosen from these samples to generate initial conditions of subsequent trajectories at constant total energy but after extra excitation in the form of additional kinetic energy deposited in the entire cluster (global excitation) or only a subpart of it (local excitation). In the latter case, we further distinguish local excitations either on the pyridinium ion or on a random water molecule. Here, we should stress that at the present temperature of interest of 100 K, the equilibrated samples generally exhibit some conformational diversity already for two or more molecules in the clusters, owing to the competing hydrogen-bond interactions between water molecules and between water and the pyridinium ion. Although we have not tried to restrict the samples to be conformation-specific, this could be a natural perspective of the present work. A large number (100 000) of such trajectories are carried out independently, taking a random excitation energy in the range of 3−8 eV. After 1 ns, each trajectory is ended, and the number and nature of the fragments are identified, the velocity distributions of the evaporated water molecules being determined for each evaporation channel.

The results (see Figure 2) show that the velocity profile strongly depends on the excitation process. At very low velocities, i.e., below 1500 m s^{-1}, each calculated velocity distribution can be accurately fitted by a Maxwell−Boltzmann distribution. In the simulations, only local excitations of water molecules can produce nonergodic high-energy components, which, as was the case for protonated water clusters,[18] seem to overestimate this effect when compared to experimental distributions, i.e., when comparing column (d) with column (a) in Figure 2. This however is not too surprising because the relative proportion of local excitations on random water molecules in the experiment is not known and thus cannot be modeled by the simulations. A first analysis (shown in blue and red in Figure 4) of the low-velocity part of the velocity

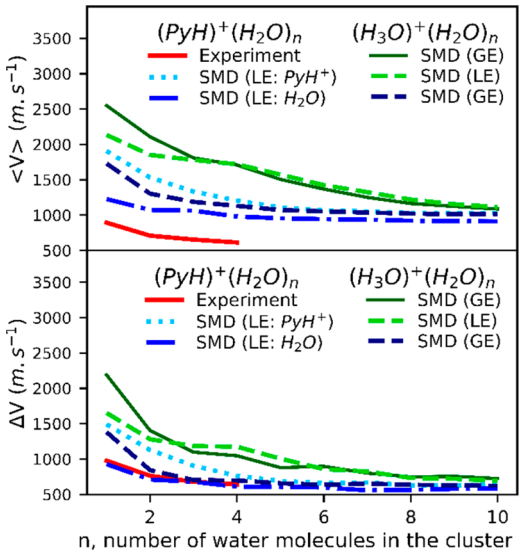

Figure 4. Average value ⟨V⟩ (upper panel) and width ΔV (lower panel) of the low-velocity part of the velocity distribution of evaporated water molecules from $PyH^+(H_2O)_{n=1-4}$ and $H_3O^+(H_2O)_n$ cluster ions. The experimental data (full red lines) are compared with the predictions of statistical molecular dynamics calculations performed for a global excitation (dashed dark blue lines), a local excitation of pyridinium (dash-dotted blue lines), or a local excitation of a random water molecule (dotted cyan lines). The results from similar simulations performed for neat protonated water clusters are also shown, assuming global excitation (dark green solid lines) or local excitation of the hydronium ion (dashed green lines).

distributions obtained from SMD simulations (given in Figure 2) shows that in the case of locally excited pyridinium a lower average value ⟨V⟩ and width ΔV are obtained than for the other excitation processes. Both quantities decrease with increasing cluster size n for each type of excitation and reach approximately constant values at large n.

Moreover, the average velocities ⟨V⟩ calculated from SMD simulations are systematically higher than the experimental values, which is due to the much shorter time window covered in those calculations (1 ns versus about 200 ns in the experiment). Longer trajectories would enable access to slower events involving lower excitation energies, associated with lower evaporation rate constants and in turn to slower

https://doi.org/10.1021/acsomega.1c06842
ACS Omega 2022, 7, 10235−10242

evaporating molecules. A global shift accounting for this difference can be applied to bring the two sets of results closer to each other, as was already noted earlier in the case of protonated water clusters, i.e., amounting to a shift of −350 m s^{-1} for local excitations on pyridine, −600 m s^{-1} for global excitations, and by −680 m s^{-1} for local excitations on water. These numbers are comparable to the value of −740 m s^{-1} reported for protonated water clusters.[25]

The SMD results corrected along these lines are compared with the corresponding data for distributions predicted for neat protonated water cluster ions (in green in Figure 4). In the latter case, the $\langle V \rangle$ and ΔV values for the low-velocity parts of the distributions are rather similar for the two types of excitations (in particular for cluster sizes above n = 3), suggesting that the low-velocity part of the distributions corresponds to molecules which are only evaporated after some redistribution of the energy from the excited molecule toward the entire cluster. In contrast, in the case of pyridinium−water cluster ions, energy deposition into the pyridinium ion leads to marked differences in the $\langle V \rangle$ and ΔV values of the low-velocity part of the distribution in particular for lower n values. However, energy deposition into a random water molecule of a pyridinium-doped water cluster ion leads to distributions, and thus $\langle V \rangle$ and ΔV values, that for larger n values are similar to the ones predicted for protonated water clusters.

These significant differences in the $\langle V \rangle$ and ΔV values for lower n values show that the low-velocity part of the distributions strongly depends on the excitation mechanism. It is interesting to note that these lower $\langle V \rangle$ and ΔV values for dissociation after initial local excitation of a pyridinium ion indicate incomplete thermalization of the deposited energy. In this case of an excitation of the pyridinium ion, which is hydrophobic and therefore located outside of the residual water cluster, only a limited amount of hydrogen bonds between the pyridinium ion and the water molecules is available to transfer the energy between both parts of the cluster. The excitation energy deposited in the molecular ion has to flow across this bottleneck in order to be transferred to the water part, leading to a more limited amount of energy available for the water molecules to evaporate.

Additional molecular dynamics simulations were performed to characterize the redistribution kinetics, by evaluating the time variations $K(t)$ of the kinetic energy in the ionic impurity after its excitation at time t = 0. Figure 5 shows the time correlation function $\langle K(t)K(0)\rangle/\langle K^2(0)\rangle$ averaged from 1000 independent trajectories and compares the results obtained for differently sized pyridinium−water cluster ions, together with earlier results obtained for the protonated water tetramer cluster ion.[29] Typical average relaxation times for the neat water clusters are on the order of some picoseconds, and times for the pyridinium−water clusters are found to lie at least one order of magnitude higher. Moreover, it is interesting to see that for these pyridinium−water cluster ions studied, the relaxation is faster for clusters containing more water molecules. This is a natural consequence of the increasingly higher probability that a water molecule is directly excited in larger clusters and to the greater number of molecules bonded to water in comparison to the pyridinium ion.

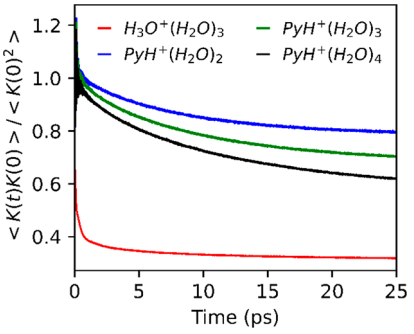

Figure 5. Normalized relaxation of the kinetic energy initially deposited in the molecular ion. The time correlations are shown for $H_3O^+(H_2O)_3$ (red line), $PyH^+(H_2O)_2$ (blue line), $PyH^+(H_2O)_3$ (green line), and $PyH^+(H_2O)_4$ (black line) upon excitation of the molecular ion at time t = 0.

The measured velocity distributions for the evaporation of a single water molecule from these pyridinium-doped water cluster ions can thus be understood in terms of two distinct contributions: the local excitation of the pyridinium ion and the local excitation of a water molecule in the cluster. We can now exploit the corresponding SMD velocity distributions to fit the experimental distributions with the two corresponding Maxwell−Boltzmann components (results shown in Figure 6),

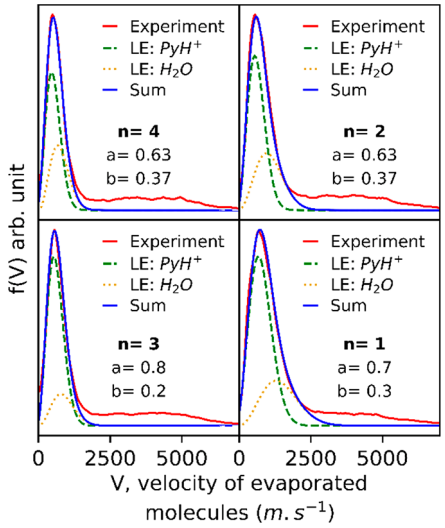

Figure 6. Velocity distributions for water molecules evaporated from pyridinium−water clusters measured in the experiment (thick red lines) and fitted distributions using two contributions from the SMD simulations assuming local excitations of either the pyridinium ion (dashed green lines) or a random water molecule (dotted orange lines). The resulting fits are shown as blue lines. The corresponding weights a (pyridinium) and b (water) are also given.

their main features (width and shift) being fixed by these SMD results (see Figure 4). To obtain the best possible fit between calculated and experimental values, we adjust the corresponding proportions of the two local excitation modes, a (pyridinium) and b (random water molecule), and the corresponding values are given in Figure 6.

It turns out that the low-velocity contribution of the experimental distributions can be fitted in this way quite well, and from the derived a and b values it follows that for the evaporation of a single molecule, the major excitation process involved is the excitation of the pyridinium ion. In contrast, and as seen below, the excitation of a water molecule is likely the cause of most events involving other evaporation channels, most notably the evaporation of several water molecules.

https://doi.org/10.1021/acsomega.1c06842
ACS Omega 2022, 7, 10235−10242

3.2. Evaporation of Several Water Molecules.

The velocity distributions corresponding to multiple evaporations of water molecules can also be determined in the present experiment. Moreover, these distributions will be interpreted here by carrying out dedicated Monte Carlo (MC) simulations of the sequential dissociation process, using SMD calculated velocity distributions for each individual evaporation step.[18] The method has been previously validated for protonated water clusters, for which a very good agreement with the experimental distributions was reached.[30] Here, we carry out MC simulations using different SMD velocity distributions as inputs corresponding to evaporations of a single molecule after local excitation either on the pyridinium ion or on a random water molecule. Figure 7 shows the velocity distribution for the

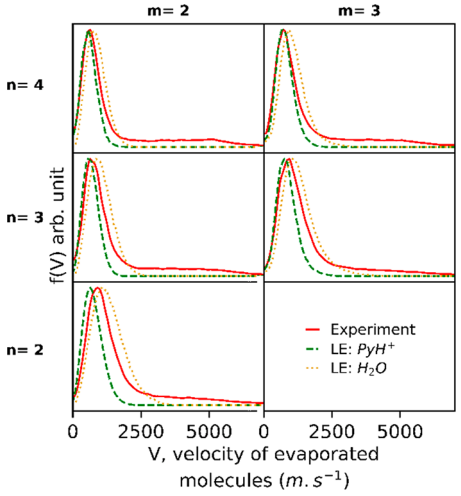

Figure 7. Velocity distributions for the sequential evaporation of two (left column) and three (right column) water molecules from $PyH^+(H_2O)_{n=2-4}$ obtained from Monte Carlo simulations based on SMD distributions for single-molecule evaporations. Full red lines: experimental data; dashed green lines: simulations assuming only local excitation of the pyridinium ion, dotted orange lines: simulations assuming only local excitation of a single random water molecule.

sequential evaporation of two (left panel) or three (right panel) molecules from $PyH^+(H_2O)_{n=2-4}$. Both kinds of excitation modes were used in the simulation as inputs: local excitation on PyH^+ in dashed green and local excitation on a water molecule in dashed yellow.

Similar results are obtained for the evaporation of two or three molecules: it can be seen that the local excitation of a random water molecule produces a wider distribution, and the corresponding maximum value lies at higher velocities than those observed in the case of a local excitation of the pyridinium ion. It is noteworthy that the discrepancies between the distributions obtained for these two excitation modes, i.e., assuming local excitations of a water molecule or the pyridinium ion, are clearly larger in the velocity distribution calculated for the evaporation of several molecules as compared to single evaporations. It should be stressed that in both experiments and these MC simulations, evaporations originate from a single-cluster atom collision, and therefore evaporation of the first and second or third molecules is all due to the same initial excitation.

Using these calculated distributions, we can again try to fit the experimental data by adjusting the proportions of the two contributions as in the case of single evaporation. As shown in Figure 8 (left panel: evaporation of two molecules, right panel: evaporation of three molecules), a good agreement between

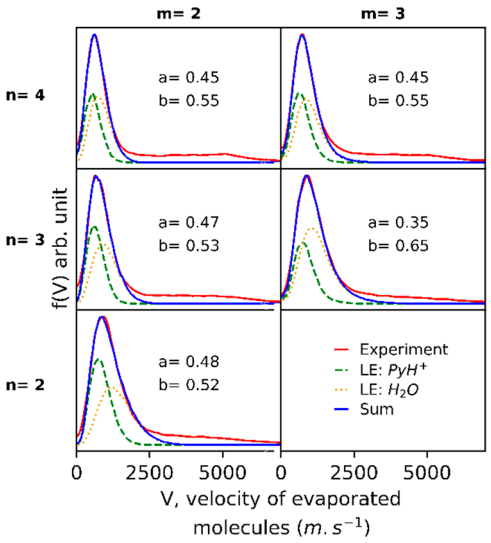

Figure 8. Experimental velocity distributions (red lines) for the evaporation of two (left column) and three (right column) water molecules from $PyH^+(H_2O)_{n=2-4}$ and fitted distributions using two contributions from the SMD simulations assuming either local excitations of a single random water molecule (dotted orange line) or local excitation of the pyridinium ion (dashed green lines). The blue lines show the sum of the two contributions. The corresponding weights a and b are also given.

calculated and experimental values can be achieved assuming approximately equal values for the two-excitation modes. Nevertheless, the contribution arising from local excitations of random water molecules is slightly more prominent for all cluster sizes studied here, and for $n = 3$ and $m = 3$, the results indicate a preference for excitation processes acting on one of the water molecules.

The results obtained here assuming sequential evaporation demonstrate that the velocity distributions measured for the evaporation of several molecules can be quantitatively reproduced from the velocity distributions corresponding to the evaporation of a single molecule. This conclusion confirms the statistical character of these events, at variance with the high-energy component which arises due to nonergodic evaporation occurring before complete thermalization.

Such a conclusion is in contrast with the earlier results obtained on protonated water clusters,[25,30] for which no such sensitivity on the type of local excitation was found in the Monte Carlo modeling in the case of multiple evaporations. The distributions measured here for a hydrophobic impurity thus suggest that some information about the initial excitation mechanisms is retained in the properties of the delayed water evaporation.

4. CONCLUSION AND OUTLOOK

We measured here the velocity distributions of evaporated molecules induced by the collision of 8 keV-$PyH^+(H_2O)_{n=1-4}$ cluster ions with argon atoms and interpreted the results using statistical molecular dynamics simulations. These SMD simulations performed with different kinds of excitations allow us to discuss the contribution of each of the excitations to the overall shape of the velocity distribution. The low

https://doi.org/10.1021/acsomega.1c06842
ACS Omega 2022, 7, 10235−10242

velocity part of the distribution can be fitted quite well by a combination of two Maxwell−Boltzmann distributions that correspond to initial excitations of a random water molecule and of the pyridinium ion, respectively. In the case of excitation on the pyridinium ion, the excitation energy deposited has to flow across a hydrogen-bond bottleneck in order to transfer toward the water part, leading to a more limited energy available for the water molecules to evaporate. The distributions measured here for a hydrophobic impurity thus suggest that information about the initial excitation mechanisms is retained in the delayed signal as evidenced by the evaporation of water molecules from these excited clusters.

The differences observed in the velocity distributions of evaporated molecules from locally excited water clusters containing hydrophilic (proton) or hydrophobic (pyridinium ion) impurities highlight the importance of the ion−molecule interactions in the competition between equilibrium and out-of-equilibrium redistribution mechanisms, a topic that has attracted significant attention in recent years (see, e.g., ref 31 and references therein). The interpretation of the experimental distribution was performed here using the results of a large number of molecular dynamics trajectories calculations undertaken assuming the collisional energy was localized into individual cluster constituents (molecules). While this assumption was justified in a dedicated earlier study,[32] the present modeling remains unable to evaluate the proportion of nonergodic events. Furthermore, it neglects reactivity and the possible occurrence of proton exchange between the pyridine and water molecules.

From the experimental perspective, it would be relevant to extend the present methodology to other molecular complexes involving larger organic building blocks. Beside the challenging context of the description of changes in the Earth's atmosphere, the method paves the way toward new investigations in the astrochemistry field.

AUTHOR INFORMATION

Corresponding Author

Michel Farizon − *Université de Lyon, Université Claude Bernard Lyon1, CNRS, IP2I Lyon/IN2P3, UMR5822, F-69622 Villeurbanne, France;* orcid.org/0000-0002-3446-6146; Email: m.farizon@ip2i.in2p3.fr

Authors

Paul Bertier − *Université de Lyon, Université Claude Bernard Lyon1, CNRS, IP2I Lyon/IN2P3, UMR5822, F-69622 Villeurbanne, France; Atomic, Molecular & Optics (AMO) Physics Laboratory, RIKEN Cluster for Pioneering Research, 351-0198 Saitama, Japan*

Léo Lavy − *Université de Lyon, Université Claude Bernard Lyon1, CNRS, IP2I Lyon/IN2P3, UMR5822, F-69622 Villeurbanne, France*

Denis Comte − *Université de Lyon, Université Claude Bernard Lyon1, CNRS, IP2I Lyon/IN2P3, UMR5822, F-69622 Villeurbanne, France; Institut für Ionenphysik und Angewandte Physik, Leopold Franzens Universität Innsbruck, 6020 Innsbruck, Austria;* orcid.org/0000-0001-7075-5941

Linda Feketeová − *Université de Lyon, Université Claude Bernard Lyon1, CNRS, IP2I Lyon/IN2P3, UMR5822, F-69622 Villeurbanne, France*

Thibaud Salbaing − *Université de Lyon, Université Claude Bernard Lyon1, CNRS, IP2I Lyon/IN2P3, UMR5822, F-69622 Villeurbanne, France*

Toshiyuki Azuma − *Atomic, Molecular & Optics (AMO) Physics Laboratory, RIKEN Cluster for Pioneering Research, 351-0198 Saitama, Japan*

Florent Calvo − *Université Grenoble Alpes, CNRS, LIPhy, F-38000 Grenoble, France;* orcid.org/0000-0002-3621-3046

Bernadette Farizon − *Université de Lyon, Université Claude Bernard Lyon1, CNRS, IP2I Lyon/IN2P3, UMR5822, F-69622 Villeurbanne, France*

Tilmann D. Märk − *Institut für Ionenphysik und Angewandte Physik, Leopold Franzens Universität Innsbruck, 6020 Innsbruck, Austria*

Complete contact information is available at: https://pubs.acs.org/10.1021/acsomega.1c06842

Funding

The authors are grateful to the LABEX Lyon Institute of Origins (ANR-10-LABX-0066) for its financial support within the program "Investissements d'Avenir" (ANR-11-IDEX-0007) of the French government operated by the National Research Agency (ANR) and to the University of Innsbruck (Leopold-Franzens-Universität Innsbruck (LFU)) for its financial support. This work was also supported by the "Groupement de Recherche Edifices Moléculaires Isolés et Environnés GDR 3533", by the joint France Japan Particle Physics laboratory (FJPPL), and by the "Mission pour les Initiatives Transverses et Interdisciplinaires" (MITI CNRS).

Notes

The authors declare no competing financial interest.

ACKNOWLEDGMENTS

We acknowledge the Institut de Physique des 2 Infinis de Lyon (IP2I) for technical support, particularly Raphaël Fillol and Roger Genre. We acknowledge the Centre de Calcul de l'Institut National de Physique Nucléaire et de Physique des Particules (CCIN2P3) for their support.

REFERENCES

(1) Contreras, C. S.; Ricketts, C. L.; Salama, F. Formation and Evolution of Circumstellar and Interstellar PAHs: A Laboratory Study. *EAS Publ* **2011**, *46*, 201−207.

(2) Parker, D. S. N.; Kaiser, R. I.; Kostko, O.; Troy, T. P.; Ahmed, M.; Sun, B. J.; Chen, S. H.; Chang, A. H. H. On the Formation of Pyridine in the Interstellar Medium. *Phys. Chem. Chem. Phys.* **2015**, *17* (47), 32000−32008.

(3) Kawaguchi, Y.; Shibuya, M.; Kinoshita, I.; Yatabe, J.; Narumi, I.; Shibata, H.; Hayashi, R.; Fujiwara, D.; Murano, Y.; Hashimoto, H.; Imai, E.; Kodaira, S.; Uchihori, Y.; Nakagawa, K.; Mita, H.; Yokobori, S.; Yamagishi, A. DNA Damage and Survival Time Course of Deinococcal Cell Pellets During 3 Years of Exposure to Outer Space. *Front. Microbiol.* **2020**, *11*, 2050.

(4) Sicilia, M. C.; Niño, A.; Muñoz-Caro, C. Mechanism of Pyridine Protonation in Water Clusters of Increasing Size. *J. Phys. Chem. A* **2005**, *109* (37), 8341−8347.

(5) Pang, X.; Ehrmaier, J.; Wu, X.; Jiang, C.; Xie, W.; Sobolewski, A. L.; Domcke, W. Photoinduced Hydrogen-Transfer Reactions in Pyridine-Water Clusters: Insights from Excited-State Electronic-Structure Calculations. *Chem. Phys.* **2018**, *515*, 550−556.

(6) Chernia, Z.; Tsori, Y. Complexation Reactions in Pyridine and 2,6-Dimethylpyridine-Water System: The Quantum-Chemical De-

scription and the Path to Liquid Phase Separation. *J. Chem. Phys.* **2018**, *148* (10), 104306.
(7) Sicilia, M. C.; Muñoz-Caro, C.; Niño, A. Theoretical Analysis of Pyridine Protonation in Water Clusters of Increasing Size. *ChemPhysChem* **2005**, *6* (1), 139−147.
(8) Esteves-López, N.; Coussan, S.; Dedonder-Lardeux, C.; Jouvet, C. Photoinduced Water Splitting in Pyridine Water Clusters. *Phys. Chem. Chem. Phys.* **2016**, *18* (36), 25637−25644.
(9) Berg, E. R.; Freeman, S. A.; Green, D. D.; Ulness, D. J. Effects of Hydrogen Bonding on the Ring Stretching Modes of Pyridine. *J. Phys. Chem. A* **2006**, *110* (50), 13434−13446.
(10) Liu, X.; Sobolewski, A. L.; Borrelli, R.; Domcke, W. Computational Investigation of the Photoinduced Homolytic Dissociation of Water in the Pyridine−Water Complex. *Phys. Chem. Chem. Phys.* **2013**, *15* (16), 5957.
(11) Bruny, G.; Eden, S.; Feil, S.; Fillol, R.; el Farkh, K.; Harb, M. M.; Teyssier, C.; Ouaskit, S.; Abdoul-Carime, H.; Farizon, B.; Farizon, M.; Märk, T. D. A New Experimental Setup Designed for the Investigation of Irradiation of Nanosystems in the Gas Phase: A High Intensity Mass-and-Energy Selected Cluster Beam. *Rev. Sci. Instrum.* **2012**, *83* (1), 013305.
(12) Berthias, F.; Feketeová, L.; Della Negra, R.; Dupasquier, T.; Fillol, R.; Abdoul-Carime, H.; Farizon, B.; Farizon, M.; Märk, T. D. Measurement of the Velocity of Neutral Fragments by the "Correlated Ion and Neutral Time of Flight" Method Combined with "Velocity-Map Imaging. *Rev. Sci. Instrum.* **2017**, *88* (8), 083101.
(13) Teyssier, C.; Fillol, R.; Abdoul-Carime, H.; Farizon, B.; Farizon, M.; Mark, T. D. A Novel ″correlated Ion and Neutral Time of Flight ″Method: Event-by-Event Detection of Neutral and Charged Fragments in Collision Induced Dissociation of Mass Selected Ions. *Rev. Sci. Instrum.* **2014**, *85* (1), 015118.
(14) Berthias, F.; Feketeová, L.; della Negra, R.; Dupasquier, T.; Fillol, R.; Abdoul-Carime, H.; Farizon, B.; Farizon, M.; Märk, T. D. Correlated Ion and Neutral Time of Flight Technique Combined with Velocity Map Imaging: Quantitative Measurements for Dissociation Processes in Excited Molecular Nano-Systems. *Rev. Sci. Instrum.* **2018**, *89* (1), 013107.
(15) Klots, C. E. Temperatures of Evaporating Clusters. *Nature* **1987**, *327* (6119), 222−223.
(16) Stace, A. J.; Shukla, A. K. The Reactions of CO_2 Cluster Ions. *Int. J. Mass Spectrom. Ion Phys.* **1980**, *36* (1), 119−122.
(17) Stace, A. J. Rotational Heating and Cooling during the Evaporation of Atoms from Excited Clusters. *J. Chem. Phys.* **1990**, *93* (9), 6502−6507.
(18) Bruni, G. Production et Caractérisation d'agrégats Moléculaires Protonés Contenant Un Nombre Donné de Molécules d'eau Auprès Du Dispositif DIAM, Ph.D. Thesis, Lyon, 2010.
(19) Teyssier, C. Spectrométrie de Masse COINTOF : Conception d'un Analyseur à Temps de Vol et Développement de La Méthode d'analyse, Ph.D. Thesis, Lyon, 2012.
(20) Berthias, F.; Buridon, V.; Abdoul-Carime, H.; Farizon, B.; Farizon, M.; Dinh, P. M.; Reinhard, P. G.; Suraud, E.; Märk, T. D. Collision-Induced Dissociation of Protonated Water Clusters. *Phys. Rev. A* **2014**, *89* (6), 062705.
(21) Berthias, F. Thermalization in a Water Nanodroplet, Ph.D. Thesis, Lyon, 2016.
(22) Hayakawa, S.; Kitaguchi, A.; Kameoka, S.; Toyoda, M.; Ichihara, T. Differences between the Internal Energy Depositions Induced by Collisional Activation and by Electron Transfer of $W(CO)_6^{2+}$ Ions on Collision with Ar and K Targets. *J. Chem. Phys.* **2006**, *124* (22), 224320.
(23) Davidson, W. R.; Sunner, J.; Kebarle, P. Hydrogen Bonding of Water to Onium Ions. Hydration of Substituted Pyridinium Ions and Related Systems. *J. Am. Chem. Soc.* **1979**, *101* (7), 1675−1680.
(24) Meot-Ner Mautner, M.; Sieck, L. W. The Ionic Hydrogen Bond. 1. Sterically Hindered Bonds. Solvation and Clustering of Protonated Amines and Pyridines. *J. Am. Chem. Soc.* **1983**, *105* (10), 2956−2961.
(25) Abdoul-Carime, H.; Berthias, F.; Feketeová, L.; Marciante, M.; Calvo, F.; Forquet, V.; Chermette, H.; Farizon, B.; Farizon, M.; Märk, T. D. Velocity of a Molecule Evaporated from a Water Nanodroplet: Maxwell-Boltzmann Statistics versus Non-Ergodic Events. *Angew. Chem.* **2015**, *54* (49), 14685−14689.
(26) Caleman, C.; Van Der Spoel, D. Evaporation from Water Clusters Containing Singly Charged Ions. *Phys. Chem. Chem. Phys.* **2007**, *9* (37), 5105−5111.
(27) Bruzzi, E.; Parajuli, R.; Stace, A. J. Reprint of "Binding Energies Determined from Kinetic Energy Release Measurements Following the Evaporation of Single Molecules from the Molecular Clusters $H^+(H_2O)_n$, $H^+(NH_3)_n$ and $H^+(CH_3OH)_n$. *Int. J. Mass Spectrom.* **2013**, *345*−*347*, 160−166.
(28) Wang, J.; Cieplak, P.; Kollman, K. A. How well does a restrained electrostatic potential (RESP) model perform in calculating conformational energies of organic and biological molecules? *J. Comput. Chem.* **2000**, *21*, 1049−1074.
(29) Feketeová, L.; Bertier, P.; Salbaing, T.; Azuma, T.; Calvo, F.; Farizon, B.; Farizon, M.; Märk, T. D. Impact of a Hydrophobic Ion on the Early Stage of Atmospheric Aerosol Formation. *Proc. Natl. Acad. Sci. U.S.A.* **2019**, *116* (45), 22540.
(30) Berthias, F.; Feketeová, L.; Abdoul-Carime, H.; Calvo, F.; Farizon, B.; Farizon, M.; Märk, T. D. Sequential Evaporation of Water Molecules from Protonated Water Clusters: Measurement of the Velocity Distributions of the Evaporated Molecules and Statistical Analysis. *Phys. Chem. Chem. Phys.* **2018**, *20* (26), 18066−18073.
(31) Ma, X.; Hase, W. L. Perspective: Chemical Dynamics Simulations of Non-Statistical Reaction Dynamics. *Philos. Trans. R. Soc. A* **2017**, *375* (2092), 20160204.
(32) Calvo, F.; Berthias, F.; Feketeová, L.; Abdoul-Carime, H.; Farizon, B.; Farizon, M. Collision-Induced Evaporation of Water Clusters and Contribution of Momentum Transfer. *Eur. Phys. J. D* **2017**, *71* (5), 110.

https://doi.org/10.1021/acsomega.1c06842
ACS Omega 2022, 7, 10235−10242